Emergent criticality in a constrained boson model

Anirudha Menon[1], Anwesha Chattopadhyay[2], Krishnendu Sengupta[1⋆] and Arnab Sen[1]

1 School of Physical Sciences, Indian Association for
the Cultivation of Science, Kolkata 700032, India
2 Department of Physics, School of Mathematical Sciences,
Ramakrishna Mission Vivekananda Educational and
Research Institute, Belur, Howrah 711202, India

⋆ ksengupta1@gmail.com

Abstract

We show, via explicit computation on a constrained bosonic model, that the presence of subsystem symmetries can lead to a quantum phase transition (QPT) where the critical point exhibits an emergent enhanced symmetry. Such a transition separates a unique gapped ground state from a gapless one; the latter phase exhibits a broken Z_2 symmetry which we tie to the presence of the subsystem symmetries in the model. The intermediate critical point separating these phases exhibits an additional emergent Z_2 symmetry which we identify. This emergence leads to a critical theory which seems to be different from those in the Ising universality class. Instead, within the data obtained from finite-size scaling analysis, we find the critical theory to be not inconsistent with Ashkin-Teller universality in the sense that the transitions of the model reproduces a critical line with variable correlation length exponent ν but constant central charge c close to unity. We verify this scenario via explicit exact-diagonalization computations, provide an effective Landau-Ginzburg theory for such a transition, and discuss the connection of our model to the PXP model describing Rydberg atom arrays.

Contents

1 Introduction

Symmetries play a pivotal role in shaping the properties of phases and phase transitions in generic many-body systems [1]. These symmetries can be global or local; the former can be spontaneously broken leading to typical symmetry-broken phases of matter such as magnets or superconductors. The local or gauge symmetries, in contrast, are always preserved [2]; however they can lead to local constraints shaping properties of low-energy phases. A well-known example of such a phenomenon involves spin-ice systems [3].

More recently, a class of symmetries which are intermediate between these two types have been identified. They manifest on $(d > 0)$-dimensional subsystems of a $(D > d)$-dimensional system and are, therefore, called subsystem symmetries. In this method of classification, the gauge (global) symmetries corresponds to $d = 0(D)$. Such subsystem symmetries play a key role in field theories which feature dimensional reduction and in physics of fractons [4–6]. It has been shown that such symmetries can be spontaneously broken [7,8].

The above-mentioned features elicit a natural question regarding role of subsystem symmetries in shaping properties of quantum phases and transitions between them. This question has been partially addressed in Ref. [9], where a quantum critical point with fractal symmetry was identified in the Newman-Moore model [10]. In addition, disordered Ising systems with subsystem symmetries are shown to have first order transitions whose properties are shaped by the presence of such symmetries [11,12].

In this work, we demonstrate, using a constrained boson model, that subsystem symmetries may change the universality class of a quantum phase transition (QPT). Our model hosts a gapped and a gapless phases separated by a QCP (Fig. 1). The gapless phase has a Z_2 symmetry-broken ground state which we show to be a consequence of the subsystem symmetry of the model. Remarkably, the intermediate QCP has an enhanced $Z_2 \times Z_2$ symmetry and belongs to the Ashkin-Teller (AT), rather than the expected Ising, universality class [13–24]. The additional Z_2 symmetry at the QCP is emergent; we identify the root of this symmetry using an effective Landau-Ginzburg theory and discuss its relation with the subsystem symmetries of the model. We explicitly compute, using exact-diagonalization (ED) on finite quasi one-dimensional (1D) arrays, the dynamical critical exponent z, correlation length exponent ν, and the entanglement entropy S_E and determine the central charge c of the conformal field theory (CFT) governing the QCP. Our analysis identifies a parameter α of the model which can be varied to access the AT critical line with variable $\nu(\alpha)$ but constant c [22,25,26]. We also discuss the relation of the boson model with the well-known PXP model describing experimentally realizable Rydberg atom arrays [27–33]. Our model leads to realization of AT criticality in a 1D model with Hilbert space dimension (HSD) ζ^L for L sites, where $\zeta = (1 + \sqrt{5})/2$ is the golden ratio. This is much smaller than HSD for other realizations of the AT model [13–24]. We therefore expect it to provide significant numerical advantage in simulating physics of AT criticality.
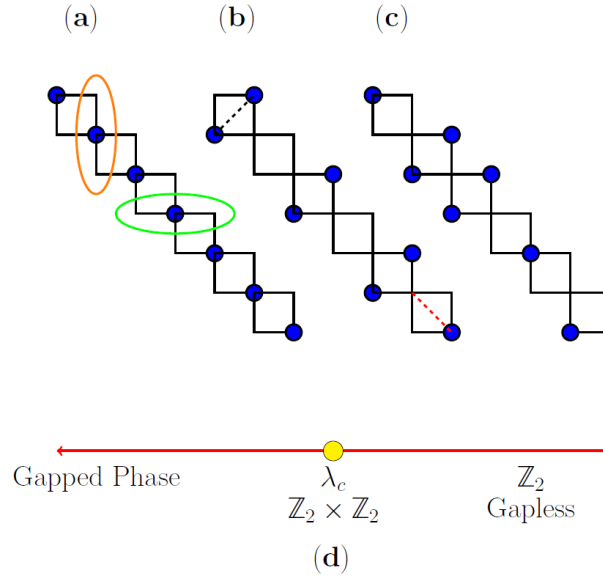
Figure 1: Schematic representation of classical Fock states of the boson model. The longitudinal(transverse) $[d_\ell(d_t)]$ diagonals are shown by dashed red (black) lines. A typical set of horizontal(vertical) connected links are shown by green(orange) ellipses. (a) Ground state at $\lambda/w \to -\infty$ for $N_p = 2n = 6$ plaquettes and total boson number $N = N_p + 1$. (b) One of the classical states forming the ground state manifold for $\lambda/w \to \infty$. (c) A state with two bosons on a vertical and a horizontal link; these are dynamically disconnected from those shown in (a) and (b). (d) Schematic phase diagram of the model as a function of λ/w showing gapped and gapless Z_2 symmetry broken phases separated by a quantum critical point (yellow circle) with enhanced $Z_2 \times Z_2$ symmetry at $\lambda = \lambda_c$. See text for details.

2 The model

We consider a model of hardcore bosons on an array of N_p square plaquettes as shown in Fig. 1. Such an array is often called as diamond chain lattice; the physics of flat bands of fermions on such a lattice have been reviewed in Ref. [34]. We shall, in what follows discuss an interacting bosonic theory on such a lattice and study its phase transition. These bosons have an additional constraint; any neighboring sites $j = (j_x, j_y)$ and $j + n = (j_x \pm 1, j_y)$ or $(j_x, j_y \pm 1)$ can not be simultaneously occupied. The longitudinal (transverse) diagonals of these plaquettes are designated by d_l (d_t). We also define the two-boson states

$$|\ell_j\rangle = b_j^\dagger b_{j+d_l}^\dagger |0_j; 0_{j+d_l}\rangle, \qquad |t_j\rangle = b_j^\dagger b_{j+d_t}^\dagger |0_j; 0_{j+d_t}\rangle. \tag{1}$$

Here $b_j^\dagger$ denotes the boson creation operator on site j of the plaquettes, $|..0_j..\rangle$ indicates a Fock state having zero bosons on site j, and we define the boson number operator to be $\hat{n}_j = b_j^\dagger b_j$. The constraint condition necessitates $\hat{n}_j \hat{n}_{j+n} = 0$ for all j. The boson Hamiltonian can then be written as $H = H_0 + H_1$ where

$$H_0 = -w \sum_j (|t_j\rangle\langle\ell_j| + \text{h.c.}),$$

$$H_1 = \lambda \sum_j (|\ell_j\rangle\langle\ell_j| - \alpha|t_j\rangle\langle t_j|), \tag{2}$$

where $w, \alpha > 0$ and λ can have either sign. We note that for $\alpha < 0$, the model can be mapped into a quantum dimer model and has an Rokhshar-Kivelson (RK) point [35, 36]; however, we shall study this model for $\alpha > 0$ where such a RK point is absent. The variation of the parameter α, as shall be elucidated later, allows one to access the AT critical line. We note that H_0 denotes a ring-exchange term for the bosons; it's implementation on a 2D square lattice is known to show strong Hilbert space fragmentation [37]. H_1 has a different sign for bosons occupying d_ℓ or d_t; this feature will be important for our purpose. In this work, we seek the phase diagram of this model as a function of λ/w and α. In what follows, we shall consider an array (Fig. 1) with open (periodic) boundary condition having even N_p plaquettes hosting $N = \sum_j n_j = N_p + (-)1$ bosons.

The model given by Eq. 2 has $[H, N] = 0$ leading to preservation of the total boson number. For open chains, the eigenstates of H, $|n_\pm\rangle$, can be labelled by their parity eigenvalues $r = \pm 1$ such that $R|n_\pm\rangle = \pm 1|n_\pm\rangle$. Here R represents reflections about an axis along d_t dividing the system in two equal halves. Importantly, R is the *only* global symmetry that can be spontaneously broken for open chains; thus, it can lead to a Z_2 broken phase. For periodic boundary conditions, the eigenstates can be labeled by momentum k along d_ℓ.

Moreover, the model has subsystem symmetry which preserves $n_0 = \sum_{j \in q} n_j$, where q denotes any vertical or horizontal link with three sites as shown in Fig. 1(a)(except the links involving the end sites of an open chain that contain only two sites) for all links. In what follows we shall work in the sector $n_0 = 1$ for all such links. We note that for $N = N_p \pm 1$, $n_0 = 1$ is the only possible subsystem symmetry sector of the model.

3 Phases of the model

In this section, we discuss the phase of H (Eq. 2) in the two limits $\lambda < 0$, $|\lambda| \gg w$ and $\lambda \gg w$ using ED in Sec. 3.1. This is followed by a perturbation theory in Sec. 3.2 which provides analytic insight into the nature of the phase for $\lambda \gg w$.

3.1 Numerical results

For $\lambda < 0$ and $|\lambda| \gg w$, the ground state of H constitutes all bosons arranged along d_ℓ as schematically shown in Fig. 1(a). The first excited state can be created by action of H_0 on one of the end sites with energy cost $\Delta E_1 = |\lambda|(2 + \alpha)$; this leads to two end states (where the plaquette with bosons on transverse diagonals is at one of the ends) shown in Fig. 2(a) for $\alpha = 1$. The action of H_0 on any of the bulk sites lead to states with $\Delta E_2 = |\lambda|(3 + \alpha) > \Delta E_1$. Thus we have an unique gapped ground state. The end states are protected from the rest of the bulk states by a finite energy gap and are therefore stable against small perturbations. The ground state entanglement entropy, S_E, shows the expected area-law behavior.

In contrast, for $\lambda \gg w$, the classical ground state manifold is $N_p/2$ fold degenerate and comprises of Fock states with maximal bosons across d_t (Fig. 1(b)). The conservation of n_0 ensures that two such plaquettes can not be neighbors; such states belong to a sector with $n_0 = 2$ on at least one vertical and horizontal links (Fig. 1(c)) and are dynamically disconnected from the $n_0 = 1$ sector. These Fock states in the $n_0 = 1$ sector can be characterized by the position of the single bosons $|j_0\rangle$ (Fig. 1(b)). We note that j_0 is either always even or always odd and can take $N_p/2$ values; this leads to a $N_p/2$-fold degenerate classical ground state manifold. This classical degeneracy is lifted by quantum fluctuations induced by H_0. The effect of H_0 can be understood within perturbation theory which we discuss in the next subsection. Here we note that the spectrum of the model, obtained using ED for a chain with $N_p = 28$ plaquettes and open boundary conditions, shows two near degenerate bands (Fig. 2(b)). For open boundary condition, the presence of the subsystem symmetry ensures a two-fold reflection symmetry R
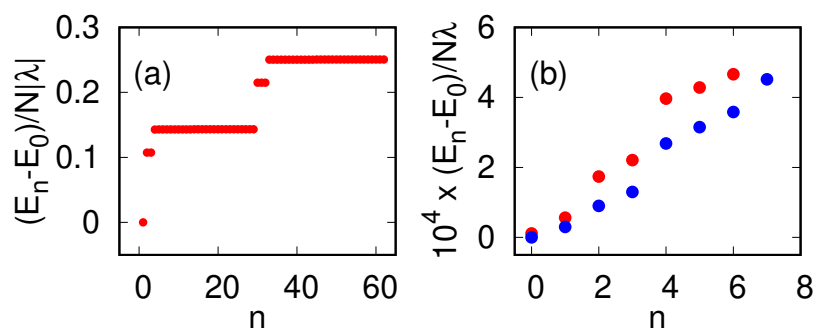
Figure 2: (a) Plot of eigenenergies of H for (a) $\lambda/w = -10$ showing the end states and the first excited state manifold and (b) $\lambda/w = 10$ showing dispersing band of eigenstates. The ground state for (b) is two-fold degenerate and gapless in thermodynamic limit. For all plots $N - 1 = N_p = 28$ and $\alpha = 1$. See text for details.

which protects this degeneracy with small energy splitting between $R = \pm 1$ states for finite N_p (Fig. 2(b)) that decrease with N_p. Thus we find a Z_2 symmetry-broken gapless ground state for $\lambda \gg w$. We have checked that S_E shows logarithmic dependence on the subsystem size ℓ_p in this phase.

3.2 Perturbation theory

In this section, we compute an effective Hamiltonian, H_{eff}, for $\lambda \gg w$ using perturbation theory which explains the properties of the ground state manifold for $\lambda \gg w$. To this end, we note that in the limit $w \to 0$ for any $\lambda/w > 0$, the ground state has $N_p/2$-fold degeneracy. To lift this degeneracy, one needs to take into account the effect of H_0. To this end, we seek a canonical transformation via an operator S which satisfies [37–39]

$$H_{\text{eff}} = e^{iS}(H_1 + H_0)e^{-iS}, \tag{3}$$

such that H_{eff} does not take one outside the low-energy manifold. Usually it is impossible to find an exact solution for S and hence H_{eff}; however, this can be achieved perturbatively and we shall chart out such a perturbative calculation where w/λ is the small parameter. In this regime, we define S such that all first order ($O(w/\lambda)$) processes that take one outside the low-energy manifold of states $|j_0\rangle$ of H_1 are eliminated. This leads to the solution [37]

$$[iS, H_1] = -H_0, \qquad H_{\text{eff}} = \frac{1}{2}[iS, H_0], \tag{4}$$

where we have omitted all processes which are $O(w^4/\lambda^4)$ or higher. To proceed further, we note that from the first relation in Eq. 4, we find that the matrix elements of S between any state $|j_0\rangle$ in the ground state manifold with energy E_0 and an excited state $|\beta\rangle$ outside this manifold with energy $E_\beta > E_0$ is given by

$$\langle \beta | iS | j_0 \rangle = \frac{\langle \beta | H_0 | j_0 \rangle}{E_\beta - E_0}. \tag{5}$$

Note that H_0 and hence S do not connect states within the low-energy manifold. Using Eq. 5 we find

$$H_{\text{eff}} = - \sum_{j_0 j_0', \beta \neq j_0, j_0'} \frac{\langle j_0 | H_0 | \beta \rangle \langle \beta | H_0 | j_0' \rangle}{E_\beta - E_0} |j_0\rangle \langle j_0'|. \tag{6}$$

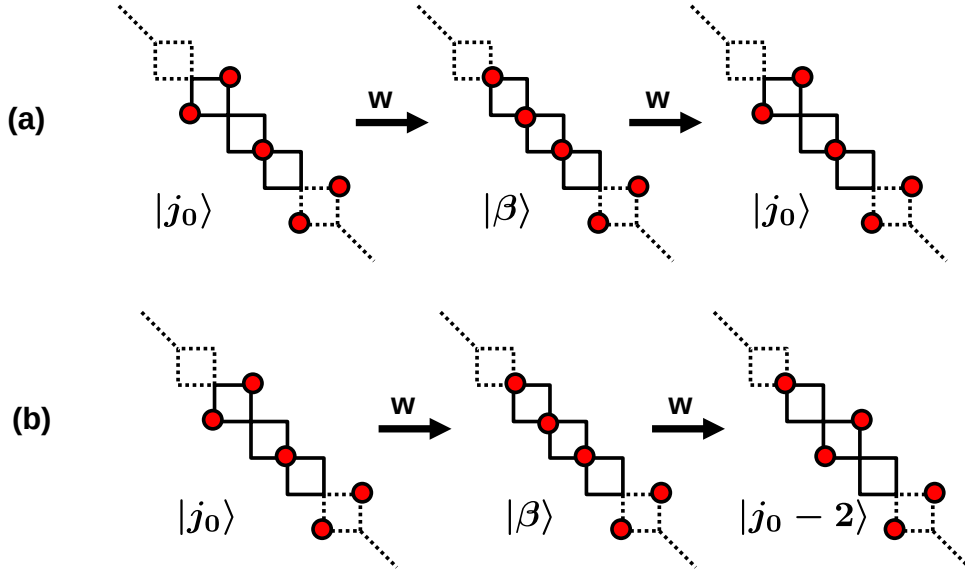This yields the leading order terms in the effective Hamiltonian.

Figure 3: (a) Schematic representation of a second-order virtual process connecting a state $|j_0\rangle$ in the ground state manifold to itself leading to renormalization of their energy. (b) Same for a process which connects $|j_0\rangle$ to $|j_0 - 2\rangle$ and thus contributes to H_{eff}. In both plots, $|\beta\rangle$ denotes a state outside the ground state manifold of H_1 with $E_\beta - E_0 = (2 + \alpha)\lambda$. The dashed blue plaquettes do not participate in the virtual process and the bosons are denoted by red circles. See text for details.

The evaluation of the matrix elements in Eq. 6 is straightforward. As explained in Fig. 3, there are two processes in the leading order. The first, schematically shown in Fig. 3(a) leads to renormalization of the energy of eigenstates in the ground state manifold and do not contribute towards lifting the degeneracy. The process which lifts this degeneracy is schematically shown in Fig. 3(b); the energy of the high-energy intermediate state for this process is $(2 + \alpha)\lambda$ leading to a matrix element of $w^2/((2+\alpha)\lambda)$. Furthermore such processes constitutes hopping of the lone boson by two lattice sites and thus connects states $|j_0\rangle$ to $|j_0'\rangle = |j_0 \pm 2\rangle$. These considerations leads to he effective Hamiltonian

$$H_{\text{eff}} = -\frac{w^2}{(2+\alpha)\lambda} \sum_{j_0} (|j_0\rangle\langle j_0 - 2| + \text{h.c.}). \tag{7}$$

The leading term in H_{eff} connects classical states where the position of the single boson is two lattice sites apart. To analyze this further, we note that chains with periodic boundary conditions and $N = N_p - 1$ shows identical behavior to open chains with $N = N_p + 1$. For the former, H_{eff} lead to energy dispersion

$$E(k) = -\frac{2w^2}{(2+\alpha)\lambda} \cos 2k + \text{O}\left(w^4/\lambda^3\right), \tag{8}$$

where we have set the length of the diagonals of the plaquette to unity. Since $E(k) = E(\pi - k)$, one has a two-fold degeneracy which can be lifted only by terms of $\text{O}(w^{N_p}/\lambda^{N_p-1})$. This degeneracy stems from the fact that in the $n_0 = 1$ sector, the dynamically connected states always have j_0 either even or odd; it is a consequence of subsystem symmetry of H.

We note that finite higher order processes do not lift the above-mentioned degeneracy. For a chain with periodic boundary condition, this is most easily seen from the fact that there are no odd-order $(\text{O}(w^{2n+1}/\lambda^{2n}))$ terms in the perturbation series which, starting from an initial state in the ground state manifold, can return to the same manifold. Thus all processes which
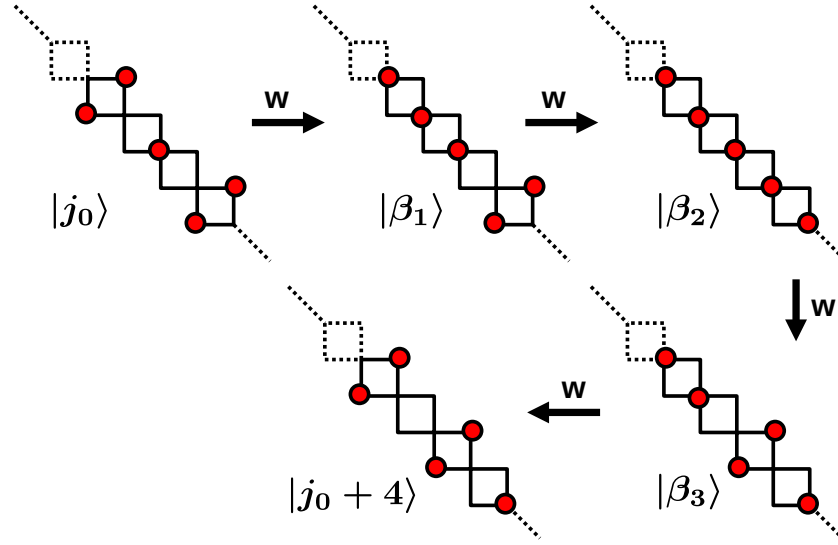
Figure 4: Schematic representation of a fourth-order virtual process connecting a state $|j_0\rangle$ in the ground state manifold to $|j_0 + 4\rangle$. Here $|\beta_1\rangle$, $|\beta_2\rangle$ and $|\beta_3\rangle$ represent excited states of H_1 with energies $(2 + \alpha)\lambda$, $(4 + 2\alpha)\lambda$, $(1 + \alpha)\lambda$ respectively with respect to the ground state manifold. All symbols are same as in Fig. 3. See text for details.

leads to finite matrix elements between states in the ground state manifold are even-ordered ($O(w^{2n}/\lambda^{2n-1})$). Next, we find that any such even-ordered term necessarily leads to shift in the position of the lone bosons by a multiple of two-sites. This follows from the fact that the lowest such term leads to a shift of this boson by two sites; one such higher order process which leads to a shift of the boson by four sites is shown in Fig. 4. Such a process connects $|j_0\rangle$ to $|j_0 \pm 4\rangle$. Similar considerations hold for all high order virtual processes; this ensures that the two-fold degeneracy is not lifted at any order by H. We also note that the gapless phase has $E_k \sim k^2$ at small k; it does not have Lorentz invariance and hence conformal invariance and does not therefore correspond to a bosonic conformal field theory.

Next we discuss the degeneracy in case of a boson array with open boundary condition. This degeneracy arises to the inversion symmetry R which, for a chain with even N_p, constitutes a reflection about a line along the transverse diagonal d_t that cuts the array into two equal halves. It is easy to see that H remains invariant under such a transformation [37]. We note that the ground state at large negative λ is an exact eigenstate of R with eigenvalue $r = 1$; however, this is not the case with classical states occupying the ground state manifold at large positive λ. Numerically, for $\lambda/w \gg 1$, we find that the ground state corresponds to a linear combination of the classical Fock state with $r = 1$. The energy gap between this state and its $r = -1$ counterpart vanishes in the thermodynamic limit leading to a two-fold degeneracy. However, for a finite size array of length N_p, a $O(N_p)$ virtual process originating from H_0 connects these states leading to a gap as can be seen from Fig. 2(c). This gap decreases algebraically with system size for the range of N_p we have numerically studied and also decreases with decreasing w/λ. We note that this behavior is in sharp contrast with that of the energy gap between the ground and the first excited state at large negative λ; the latter remains stable in the thermodynamic limit and does not show appreciable change with increasing N_p.
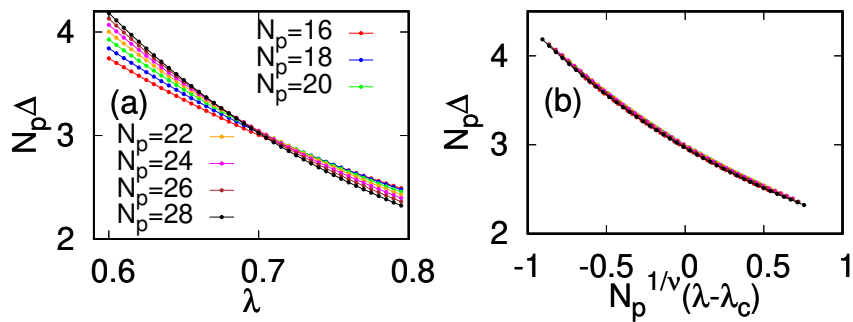
Figure 5: (a) Plot of ΔN_p as a function of λ obtained using ED; the curves cross at $\lambda = \lambda_c \simeq 0.7$ indicating $z = 1$. (b) Plot of ΔN_p as a function of $N^{-1/\nu}(\lambda - \lambda_c)$ leading to optimal scaling collapse for $\nu \simeq 1.53211 \pm 0.01246$ and $\lambda_c/w \simeq 0.69$. For all plots $N - 1 = N_p = 28$ and $\alpha = 1$. See text for details.

4 Quantum critical point

The ground state of the boson model for $\lambda \gg w$ breaks a Z_2 symmetry. In contrast, that for $\lambda < 0$ and $|\lambda| \gg w$, does not break any symmetry. Thus it is excepted that these states will be separated by a phase transition. In this section, we investigate this transition in details. Our numerics on finite chain with $N_p \leq 28$, in Sec. 4.1, demonstrates that the transition, in contrast to the expected Ising, belongs to the AT universality class; the critical point hosts an additional emergent Z_2 symmetry. In Sec. 4.2, we provide a Landau-Ginzburg theory for the transition which provides an analytic understanding of the mechanism for the additional emergent symmetry.

4.1 Numerical results

In this section, we present our results on numerical computation of the exponent ν, the entanglement entropy S_E and the central charge c of the boson system at the critical point. To investigate the nature of this QCP between the Z_2 symmetry broken ground state at $\lambda > 0$ and the unique ground state at $\lambda < 0$, we carry out standard finite-size scaling analysis using ED for the boson chain with open boundary condition. The results obtained from such a study is shown in Figs. 5, 6, and 7.

It is well-known that the smallest energy gap $\Delta \equiv \Delta_{10} = (E_1 - E_0)$ (E_{n-1} denotes the nth energy eigenvalues) for a finite chain near the critical point satisfies [40]

$$\Delta = N_p^{-z} f\left(N_p^{1/\nu}(\lambda - \lambda_c)\right), \tag{9}$$

where f denotes a scaling function, z is the dynamical critical exponent, ν is the correlation length exponent and λ_c is the critical value of λ. Our results, shown in Fig. 5 for a representative value $\alpha = 1$, indicate an excellent match with the above form of Δ for $z = 1$ and $\nu = 1.53211 \pm 0.01246$. Similar matches were found for other values of α; the $\alpha \to \infty$ limit, as we shall see in the next section, constitutes a realization of the PXP model and will be separately discussed in Sec. 5. The value of ν found in Fig. 5 is clearly inconsistent with expected Ising universality class; in contrast, it is consistent with AT universality.

To further confirm that this transition is distinct from its Ising counterpart, we first note that a QCP which belongs to AT universality with $Z_2 \times Z_2$ symmetry is expected to have three gapless modes at λ_c; consequently, $\Delta_{20}N_p$ and $\Delta_{30}N_p$ is also expected to show finite-size scaling behavior similar to Δ. This distinguishes such a critical point from one with Ising
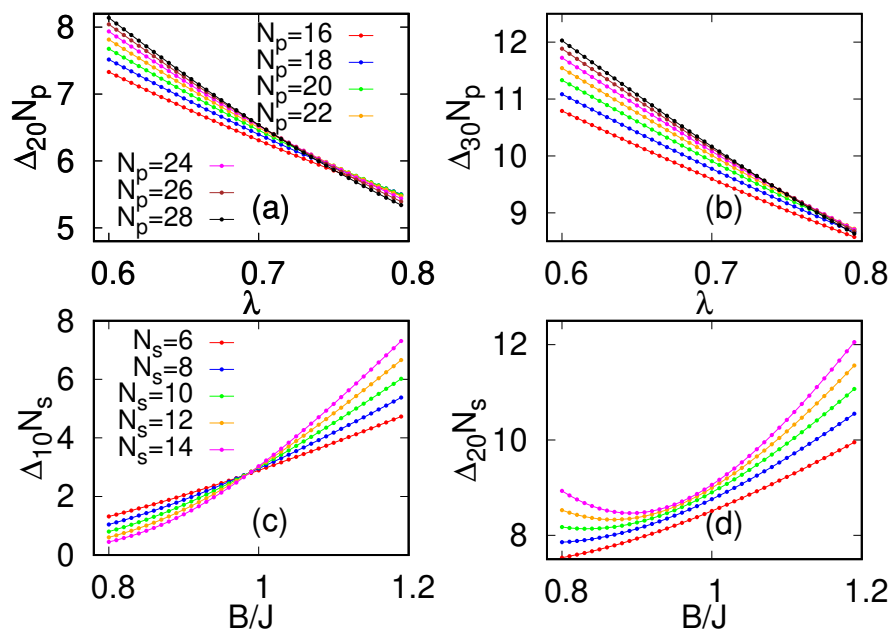
Figure 6: Plot of (a) $\Delta_{20}N_p$ (a) and (b) $\Delta_{30}N_p$ as a function of λ showing crossings at $\lambda_c/w = 0.70925 \pm 0.00636$ and 0.74544 ± 0.0273375 respectively. (c) and (d) In contrast, the Ising model shows such crossing only for $\Delta_{10}N_p$ as a function of J/B but not for $\Delta_{20}N_p$. See text for details.

symmetry. Thus a signature of the AT universality may be found by studying scaling behavior of the higher energy gaps near the critical point. To this end, we define the gap $\Delta_{n0} = E_n - E_0$ and plot $\Delta_{20}N_P$ and $\Delta_{30}N_p$ (where N_p denotes the number of plaquettes) as a function of λ (Figs. 6(a) and (b)). These plots indicate the presence of a crossing although the position of the crossing point shifts towards larger value of λ. This can be attributed to finite-size effect since the scaling behavior of these higher gaps is expected to have stronger system size dependence leading to a strong finite-size shift of the crossing points towards larger λ. In contrast, similar results for Ising criticality, obtained by performing ED on an Ising chain with

$$H_{\text{Ising}} = -J \sum_{\langle ij \rangle} \sigma_i^z \sigma_j^z - B \sum_j \sigma_j^x, \tag{10}$$

does not show any crossing for Δ_{20}; only Δ_{10} shows this feature at $J/B = 1$ (Figs. 6(c) and (d)). The behavior of the latter plots (Figs. 6(c) and (d)) is qualitatively distinct from the former (Figs. 6(a) and (b)). This analysis therefore distinguishes the present critical point from its Ising counterpart.

To ascertain AT universality of the transition and to explore the role of the parameter α, we obtain $\nu(\alpha)$ using finite-size scaling; the resultant plot is shown in Fig. 7(a). We find that varying α leads to a range of ν; ν increase with decreasing α with $\nu \sim 3$ for $\alpha = 0$ and $\nu \rightarrow 1.24$ as $\alpha \rightarrow \infty$. This indicates that varying α allows one to access a section of the AT critical line; we note that in the microscopic Ashkin-Teller model $2/3 \leq \nu < \infty$ on the critical line; the two limits correspond to the 4-state Potts ($\nu = 2/3$) and the Kosterliz-Thouless universality class ($\nu \rightarrow \infty$) respectively. The corresponding phase diagram (Fig. 7(b)) shows the position of this line in the $\lambda - \alpha$ plane.
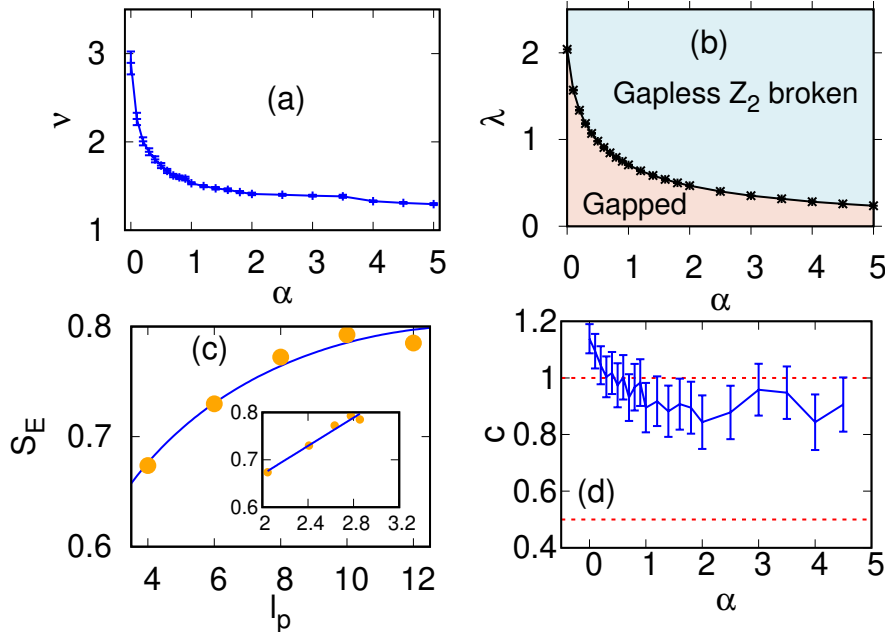
Figure 7: (a) Plot of ν as a function of α. (b) Phase diagram in $\lambda-\alpha$ plane showing the AT critical line. (c) Plot of S_E as a function of l_p for $\alpha = 1$ showing logarithmic dependence of S_E on l_p; the inset show a plot of S_E as a function of $\ln[(2N_p/\pi)\sin(\pi l_p/N_p)]$ leading to $c = 0.895072 \pm 0.08725$. (d) Plot of c as a function of α. The red dotted lines indicate $c = 1$ and $c = 1/2$. See text for details.

Another feature of the AT critical line is that the central charge of the critical theory describing the transition remains fixed to $c = 1$ on the entire line. To further confirm that the QCPs on the line conform to AT universality, we therefore compute S_E as a function of the subsystem size l_p at $\lambda = \lambda_c$ and for $\alpha = 1$. This computation is carried out using standard methods in the literature [41,42] and may be summarized as follows.

We partition the boson ladder of length L along its longitudinal diagonal into subsystems A of length ℓ_A and B of length ℓ_B. The ground state of the system is then represented by

$$|\psi\rangle = \sum_{i,\mu} c_{i,\mu} |i,\mu\rangle, \tag{11}$$

where the labels i and μ correspond to subsystems A and B respectively. As discussed in Refs. [41,42], one needs to carry out this partitioning in a manner consistent with all the constraint conditions of the model. The density matrix for the ground state can then be written as

$$\rho = |\psi\rangle \otimes \langle\psi| = \sum_{ij}\sum_{\mu\nu} c_{i\mu}^* c_{j\nu} |[i][\mu]\rangle \otimes \langle[j][\nu]|, \tag{12}$$

where $[i]$, $[j]$ represent the set of indices associated with subsystem A and $[\mu]$ and $[\nu]$ with subsystem B. The $c_{i\mu}$'s are the components of the ground state wavefunction in the Fock basis. To compute the entanglement entropy, we need to trace over the

$$\rho_A = Tr_B(\rho) = \sum_{\sigma}\sum_{ij}\sum_{\mu\nu} c_{i\mu}^* c_{j\nu}\delta_{\mu\sigma}\delta_{\nu\sigma} |[i]\rangle \otimes \langle[j]|. \tag{13}$$

This yields $\rho_A^{ij} = \sum_{\sigma} c_{i\sigma}^* c_{j\sigma}$. The von-Neuman entanglement entropy is defined in terms of ρ_A as

$$S_E = -tr[\rho_A \ln \rho_A]. \tag{14}$$

Denoting the eigenvalues of ρ_A to be $\{\lambda_i\}$, one can compute $S_E = -\sum_i \lambda_i \ln \lambda_i$. In this work, we have used this formalism to compute the entanglement entropy $S_E(\ell_A)$ for which $\ell_A = L - \ell_b = \ell$.

A plot of S_E, shown in Fig. 7(c), shows a logarithmic dependence of S_E as a function of l_p which is consistent with the Cardy-Calabrese result [25, 26]

$$S_E = (c/6)\ln\left[\left(2N_p/\pi\right)\sin\left(\pi l_p/N_p\right)\right]. \tag{15}$$

This allows one to extract the central charge c of the conformal field theory governing the critical point (inset of Fig. 7(c)); we obtain $c = 0.895072 \pm 0.08725$ for $\alpha = 1$. Similar computations for other α shows that c stays close to unity on the line; a plot of c as a function of α, shown in Fig. 7(d), demonstrates this fact. We note here that since our ED can access at most $N_p = 28$, it only provides subsystems with $l_p = 4, 6, 8, 10$ and 12. Thus the systematic error in the extraction of c is higher compared to ν and λ_c; however, even with this constraint, the central charge seems to be not inconsistent, within error bars as indicated in Fig. 7(d), with AT universality [23, 24, 43]. It is clearly different from that of an Ising transition for which $c = 1/2$.

4.2 Landau-Ginzburg theory

The AT universality class hosts a $Z_2 \times Z_2$ symmetry. In this section, we provide a possible explanation for the origin of the additional emergent Z_2 symmetry at the QCP in our model. We show that this phenomenon can be understood from a Landau-Ginzburg (LG) theory for the transition. We stress that this does not mean that the universality class of the transition can be completely determined using such an approach; this usually requires a renormalization group analysis which is impossible to carry out analytically for interacting field theories in $d = 1$. However, even without such a calculation, a basic analysis of the interaction terms of the model based on underlying symmetry of the Hamiltonian may provide useful information about possible symmetries of the critical point. This symmetry based approached has been used in Refs. [44] and [45] in context of different models.

The ground state at $\lambda > \lambda_c$ is two-fold degenerate and at the QCP, a state from the excited state manifold crosses the ground state. The degeneracy ensures that if such a crossing occurs, for a periodic chain, at a momentum k_0 ($-\pi \le k_0 \le \pi$), there must be an analogous crossing at $\pi - k_0$. The critical theory, is therefore governed by a bosonic low-energy field [44, 45]

$$\Phi(x, t) = e^{ik_0 x}\varphi_1(x, t) + e^{i(\pi - k_0)x}\varphi_2(x, t), \tag{16}$$

where φ_1 and φ_2 are the low-energy fluctuations around k_0 and $\pi - k_0$ respectively. The invariance of the $\Phi(x, t)$ under $k_0 \to \pi - k_0$ implies that $\varphi_{1(2)} \to \varphi_{2(1)}$ under such a transformation. An effective LG theory which respects this symmetry can be written in terms of $\varphi_{1,2}(x, t)$ as

$$\mathcal{L} = \sum_{\alpha=1,2}\left(|\partial_\mu \varphi_\alpha|^2 + r|\varphi_\alpha)|^2\right) + c_1\left(|\varphi_1|^4 + |\varphi_2|^4\right) + c_2|\varphi_1|^2|\phi_2|^2 + c_3\left(\varphi_1^*\varphi_2 + h.c.\right)^2, \tag{17}$$

where $c_1 > 0$ and we have suppressed the space time labels of $\varphi_{1,2}$ for clarity.

At QCP $r = 0$ and Eq. 17 predicts two possible scenarios. The first is that only one of the two fields condense. This happens when if $c_3 > 0$ and $c_2 > 0$ or if $c_3 < 0$ but $c_2 + 2c_3 > 0$. In this case the critical theory can be described by a standard Landau functional involving a single scalar field. In contrast, if either $c_2 + 2c_3 < 0$ and $c_3 < 0$ or $c_2 < 0$, both φ_1 and φ_2 condenses. For both of these latter possibilities, $\mathcal{L}$ is two-fold degenerate; it remains invariant under $\theta_0 \to \pi - \theta_0$, where θ_0 is the relative phase between φ_1 and φ_2. Its minima corresponds to $\theta_0 = 0, \pi$ for $c_3 < 0$ and $\theta_0 = \pi/2, 3\pi/2$ if $c_3 > 0$. This leads to an *additional emergent*

Z_2 symmetry. Our analysis indicates that the microscopic Z_2 symmetry of the gapless phase at $\lambda > 0$, which derives its root from the subsystem symmetry of the model, necessitates a $\mathcal{L}$, with two low-energy fields; it is therefore a necessary (but not sufficient) requirement for the emergent Z_2 symmetry at the QCP.

5 Mapping to a 1D spin model

In this section, we present the mapping of H model to a modified PXP Hamiltonian [31–33, 46, 47]. It is well known that PXP models provide a description of the low-energy physics of ultracold Rydberg atoms [27–29, 31–33, 46, 47]; we show that our model reduces to the PXP model for $\alpha \to \infty$ thus allowing for possible experimental relevance of the phase transition studied in the original boson model.

To this end, we first map a state with two bosons on the transverse diagonal d_t of a plaquette to a up-spin at its center as shown in Fig. 8(a): $|t_j\rangle \to |\uparrow_{x_j}\rangle$, where x_j denotes the coordinate of the center of the plaquette. Similarly, a state with two bosons on the longitudinal diagonal d_ℓ of a plaquette is mapped to a down-spin: $|\ell_j\rangle \to |\downarrow_{x_j}\rangle$ (see Fig. 8(b)). Crucially, the presence of subsystem symmetry does not allow states with two neighboring plaquettes each having two bosons on d_t; such a state correspond to $n_0 = 2$ and are dynamically disconnected from states with $n_0 = 1$. This allows one to realize the PXP constraint of not having two neighboring up-spins. Finally, as shown in Fig. 8(c), we denote a lone boson on in a given plaquette as an unflippable down spin since the action of H_0, in contrast to the standard down-spins defined earlier, can not flip it.

To express the boson Hamiltonian in terms of these spins we define the following operators

$$\tau^z_{x_j} = |t_j\rangle\langle t_j| - |\ell_j\rangle\langle \ell_j|, \qquad \tau^x_{x_j} = |t_j\rangle\langle \ell_j| + |\ell_j\rangle\langle t_j|. \tag{18}$$
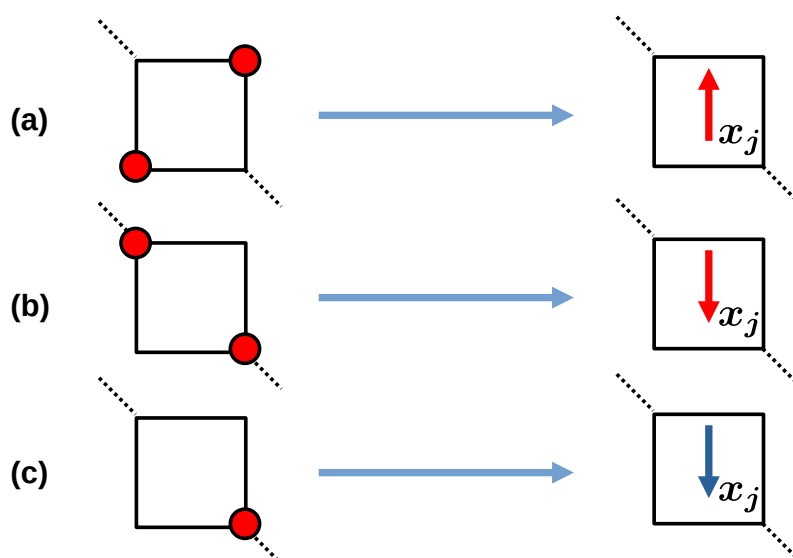

Figure 8: Schematic representation of mapping of bosons to PXP spins. (a) A boson state with two bosons on the transverse diagonal is mapped to an up spin at the center of the plaquette with coordinate x_j. (b) A boson state with two bosons on the longitudinal diagonal is mapped to a flippable down spin. (c) A lone boson is mapped to an unflippable down spin. See text for details.
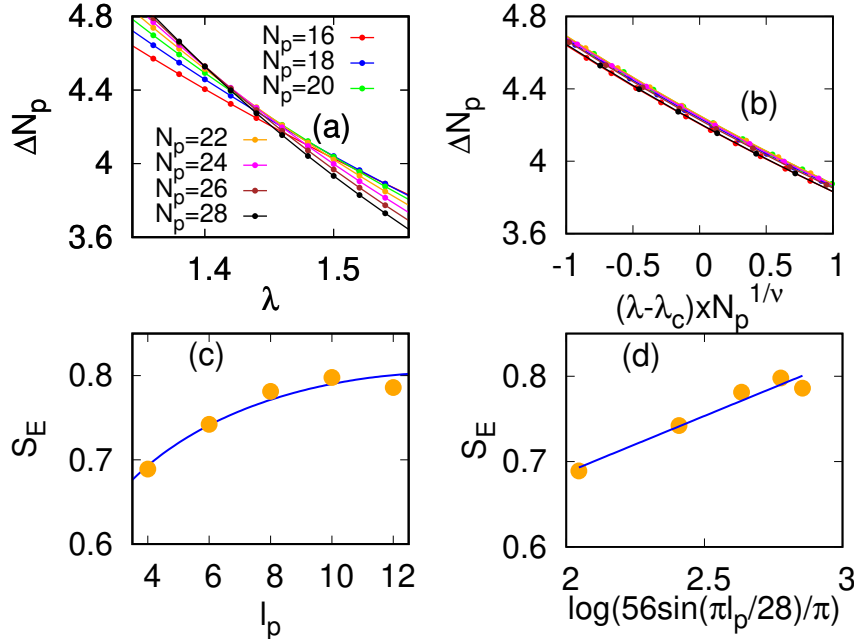
Figure 9: Finite-size scaling analysis for $\alpha \to \infty$ starting from H' (Eq. 21). (a) Plot of ΔN_p as a function of λ; the curves cross at $\lambda = \lambda_c \simeq 1.45097 \pm 0.002631$ indicating $z = 1$. (b) Plot of ΔN_p as a function of $N^{-1/\nu}(\lambda - \lambda_c)$ leading to optimal scaling collapse for $\nu \simeq 1.24173 \pm 0.02461$. (c) Plot of S_E as a function of l_p showing logarithmic dependence of S_E on l_p (d) Plot of S_E as a function of $\ln[(2N_p/\pi)\sin(\pi l_p/N_p)]$ leading to 0.797501 ± 0.1052. For all plots $w = 1$. See text for details.

We also define a projection operators $P_{x_j} = (1 - \tau^z_{x_j})/2$ which projects to $|\downarrow_{x_j}\rangle$. Noting that a flip of spin from down to up is possible only if the neighboring sites also have down spins (either flippable or unflippable), we can write

$$H_0 = -w \sum_{x_j} \tilde{\tau}^x_{x_j}, \qquad \tilde{\tau}^x_{x_j} = P_{x_j-1} \tau^x_{x_j} P_{x_j+1}. \tag{19}$$

To write H_1 in terms of spin operators, we note that H_1 does not count unflippable spins. Thus we need to count only flippable down spins. It is easy to see from the boson states such spins are the ones which are flanked by two other down spins on neighboring sites. These considerations lead one to the spin Hamiltonian

$$H_1 = -\lambda \sum_{x_j} \left(\alpha \frac{1 + \tau^z_{x_j}}{2} - P_{x_j-1} \frac{1 - \tau^z_{x_j}}{2} P_{x_j+1} \right)$$

$$= -\lambda \sum_{x_j} \left(\alpha \tau^z_{x_j}/2 - P_{x_j-1} P_{x_j} P_{x_j+1} \right), \tag{20}$$

where in the second line, we have ignored an irrelevant constant. We note that the last term in Eq. 20 which arises due to the presence of unflippable down spins (or lone bosons in a plaquette) distinguishes the model from the PXP model in a magnetic field [45].

Next, we study the limit $\alpha \to \infty$ with $\lambda \alpha / w$ being held fixed and kept finite. In this limit, one can ignore the last term in Eq. 20 and map the plaquette boson model to the PXP model in a magnetic field. This yields a spin Hamiltonian H' given by

$$H' = -\sum_j \left(w \tilde{\tau}^x_{x_j} + \lambda \tau^z_{x_j} \right), \tag{21}$$

where $\lambda \to \lambda\alpha/2$. Such a chain with periodic boundary condition (PBC) has been studied in detail [45,47] and is known to have Ising critical point at $\lambda_c/w \simeq 1.31$. However, the criticality in the model with open boundary condition (OBC) turns out to be different. One of the sources of this difference stems from the nature of the ground state at large λ/w. The PXP chain with PBC has a gapped ground state at large λ/w; in contrast, in the presence of OBC, the ground state at large λ/w is gapless. Such a gapless states occurs due to superposition of all Fock states with alternate up and down spins along with a single domain wall. Note that the presence of such a domain wall in the ground state sector can be traced back to the presence of subsystem symmetry of the original boson Hamiltonian, which, for a given $N = N_p + 1$, necessitates the presence of a lone boson in the ground state manifold. The energy band of these excited states has a width $\sim 1/\alpha$ as can be deduced from Eq. 7.

A finite-size scaling analysis starting from H' confirms the difference in criticality of the PXP chain with OBC from the one with PBC. This is shown in Fig. 9. Our analysis indicates a strong finite size effect for a chain with OBC at large α; this feature is to be distinguished from the chain with PBC and may arise from the difference in nature of the ground states in the two cases at large λ/w. Our numerical results, shown in Figs. 9(a) and (b) indicate $\lambda_c/w = 1.45097 \pm 0.002631$, and $\nu = 1.24173 \pm 0.02461$. Fig 9(c) shows a plot of S_E, computed using similar methods as in Sec. 4.1. A fit of S_E using Eq. 15 yields $c = 0.797501 \pm 0.1052$ which is quite different from Ising universality; these exponents are however, consistent with AT universality after allowing for strong finite-size corrections for estimation of c at large α. At finite α, the third term provides an additional three-site interaction which changes ν; such a multi-spin term therefore provides a way to access the AT line in these experimentally realizable Rydberg systems [27–30]. Engineering such terms in Rydberg arrays requires further work which we leave for future studies.

6 Discussion

In this work, we have studied a boson model with subsystem symmetry and have shown that the presence of such subsystem symmetry can change the universality of the quantum phase transition of the model. Our analysis indicates that the model has two phases; one of them occurs at large negative λ and is gapped. The second phase, occurring at large positive λ is gapless in the thermodynamic limit; moreover, it breaks a discrete Z_2 symmetry. Our analysis unravels the key role played by the subsystem symmetry behind the presence of the latter phase. We note here that our reference to subsystem symmetry comes from the 2D version of this model analyzed in Ref. [37] where the role of subsystem symmetry has been discussed. In this work, where we consider the bosons with a slightly modified Hamiltonian on a two-leg ladder (diamond chain lattice), the subsystem symmetry of the 2D lattice model gets translated into conservation of bosons number in any vertically or horizontally connected sites. When we discuss this in the 1D spin chain language in Sec. 5, this symmetry leads to the constraint condition of not having neighboring up spins.

We note that the boundary condition play a crucial role in such constrained systems. This is most easily understood in the spin language. The boson model has been exactly mapped to a 1D PXP model with additional interaction term in Sec. 5. We find that this model has completely different ground state manifolds for periodic and open boundary conditions when $\lambda \gg w$. This is most easily seen in the limit $\alpha \to \infty$ with $\lambda\alpha/w$ held finite. Here the model reduces to a 1D PXP spin chain studied earlier [46,47]. For PBC, the ground state manifold consists of two Fock states given by $|1, 0, 10, ...1, 0\rangle$ and $|0, 1, 0, 1..0, 1\rangle$ where 1(0) represent an up(down) spin. The choice of one of these two states leads to a Z_2 broken ground state. The transition from the gapped unique ground state for $|\lambda| > w$ and $\lambda < 0$ to such a Z_2

symmetry broken state therefore belongs to the Ising universality class as shown earlier [46]. In contrast, for OBC, the ground state manifold contains, in addition to the two states mentioned above, O(L) domain wall Fock states; one such typical state, for example, is given by $|1,0,0,1,0,1,...0,1\rangle$. Note such a state is prohibited for a PXP chain with PBC due to the constraint. To verify this, we have computed the structure factor S_q for a N site spin chain: $S_q = \langle \psi_q^* \psi_q \rangle$, where $\psi_q = (1/N)\sum_j n_j e^{i2\pi j/q}$ and $n_j = (1+\sigma_j^z)/2$ counts the number of up-spins on each site. For a PXP chain with periodic boundary condition $S_{q=2}$ saturates to 1/4 in the thermodynamic limit as suggested by $1/N$ extrapolation performed with data for $N \leq 26$; however in the presence of constraint and open boundary condition, a similar analysis shows that $S_q|_{N\to\infty} \sim 0.034$. This confirms the different nature of the ground state at large positive $\lambda/w = 14$ for periodic and open boundary conditions; for the present model, our analysis suggests that the latter leads to a gapless ground state. This provide a concrete example that the bulk phase may change due to boundary condition in a constrained spin or boson model; the situation is in contrast to that of unconstrained models where boundary conditions usually do not have drastic effect on bulk phases.

These two phases of the model, as expected, are separated by a quantum critical point. The universality class of this critical point depends on the nature of the phases it separates. For a chain with PBC, we find the critical point to belong to the expected Ising universality class. However, in contrast to the standard expectation, we find, within the system size accessible in our numerics, that the universality class of the transition with OBC is not Ising. This change in universality class may originate from the change in nature of the bulk phase for $\lambda \gg w$; the transition occurs from an unique gapped to a gapless, rather than a gapped Z_2 symmetry broken, phase in the present spin model (Eq. 19 and 20) with open boundary condition.

Our numerics indicate that the critical point may belong to the AT universality class. The parameter α of the model (Eq. 2) can be tuned to access a critical line with variable ν but constant c; this behavior, within the system sizes that we could access, is consistent with AT criticality. Our analysis indicates that the boson model can access a part of this AT critical line $(3 \leq \nu \leq 1.24)$. The computed central charge shows strong fluctuation; this is due to the fact that using ED, one can access $N_P \leq 28$ allowing subsystem sizes $4 \leq \ell_p \leq 12$. However, even with this constraint, the values of c obtained seem to be very different from its value for Ising criticality ($c = 1/2$). Moreover, the tunability of ν along with a value of $c \neq 1/2$ certainly seems to suggest that for the system sizes accessible by ED, the universality class of the transition is not inconsistent with Ashkin-Teller. However accessing larger system sizes is necessary for a more definitive conclusion. In this respect we note that while the presence of the constraint does not allow a straightforward numerical analysis of this model using standard density-matrix-renormalization group (DMRG) or Quantum-Monte-Carlo (QMC) methods, certain recent methods using sweeping cluster QMC algorithm [48] or DMRG of constrained dimer model [49] may prove useful. These endeavors constitute future directions of research.

Our mapping of the boson model to the PXP spin model in a magnetic field with open boundary condition leads to a possibility of its realization in an ultracold Rydberg atom chain. The two models are identical in the limit $\alpha \to \infty$ with $\lambda\alpha/w$ held fixed and finite. For finite α, we find that the boson model is equivalent to a PXP model in a magnetic field together with an additional three-spin term. The variation of the strength of this three-spin term (which is same as varying α keeping λ/w fixed) allows one to access the AT critical line. The realization of such a three spin term in experimental Rydberg platforms may be of future interest.

The Hilbert space dimensions (HSD) of H_s and hence H scales as ζ^L; H_s therefore provides easier numerical access to the physics of the AT critical line compared to a standard spin model with HSD 4^L [50, 51]. This may be useful for studying non-equilibrium quantum dynamics of the model across the AT critical line; this might be another subject for future study [41, 42].

In conclusion, we have demonstrated the emergence of AT criticality in a constrained bosonic model with subsystem symmetry. We point out the crucial role of subsystem symmetries in determining the universality class of the critical theory. Our analysis also shows that the model is closely related to the well-known PXP model relevant for Rydberg atom arrays and forms the most convenient platform for numerical studies of the AT critical line.

Acknowledgments

References

[1] P. W. Anderson, *Basic notions of condensed matter physics*, CRC Press, Boca Raton, USA, ISBN 9780429494116 (2018), doi:10.4324/9780429494116.

[2] S. Elitzur, *Impossibility of spontaneously breaking local symmetries*, Phys. Rev. D **12**, 3978 (1975), doi:10.1103/PhysRevD.12.3978.

[3] C. Nisoli, R. Moessner and P. Schiffer, *Colloquium: Artificial spin ice: Designing and imaging magnetic frustration*, Rev. Mod. Phys. **85**, 1473 (2013), doi:10.1103/RevModPhys.85.1473 [preprint doi:10.48550/arXiv.1306.0825].

[4] A. Gromov and L. Radzihovsky, *Colloquium: Fracton matter*, Rev. Mod. Phys. **96**, 011001 (2024), doi:10.1103/RevModPhys.96.011001.

[5] R. M. Nandkishore and M. Hermele, *Fractons*, Annu. Rev. Condens. Matter Phys. **10**, 295 (2019), doi:10.1146/annurev-conmatphys-031218-013604.

[6] M. Pretko, X. Chen and Y. You, *Fracton phases of matter*, Int. J. Mod. Phys. A **35**, 2030003 (2020), doi:10.1142/S0217751X20300033 [preprint doi:10.48550/arXiv.2001.01722].

[7] C. D. Batista and Z. Nussinov, *Generalized Elitzur's theorem and dimensional reductions*, Phys. Rev. B **72**, 045137 (2005), doi:10.1103/PhysRevB.72.045137 [preprint doi:10.48550/arXiv.cond-mat/0410599].

[8] Y. You, T. Devakul, F. J. Burnell and S. L. Sondhi, *Subsystem symmetry protected topological order*, Phys. Rev. B **98**, 035112 (2018), doi:10.1103/PhysRevB.98.035112 [preprint doi:10.48550/arXiv.1803.02369].

[9] Z. Zhou, X.-F. Zhang, F. Pollmann and Y. You, *Fractal quantum phase transitions: Critical phenomena beyond renormalization*, (arXiv preprint) doi:10.48550/arXiv.2105.05851.

[10] J. P. Garrahan and M. E. J. Newman, *Glassiness and constrained dynamics of a short-range nondisordered spin model*, Phys. Rev. E **62**, 7670 (2000), doi:10.1103/PhysRevE.62.7670 [preprint doi:10.48550/arXiv.cond-mat/0007372].

[11] G. Canossa, L. Pollet, M. A. Martin-Delgado, H. Song and K. Liu, *Exotic symmetry breaking properties of self-dual fracton spin models*, Phys. Rev. Res. **6**, 013304 (2024), doi:10.1103/PhysRevResearch.6.013304 [preprint doi:10.48550/arXiv.2311.11066].

[12] B. Rayhaun and D. Williamson, *Higher-form subsystem symmetry breaking: Subdimensional criticality and fracton phase transitions*, SciPost Phys. **15**, 017 (2023), doi:10.21468/SciPostPhys.15.1.017 [preprint doi:10.48550/arXiv.2112.12735].

[13] J. Ashkin and E. Teller, *Statistics of two-dimensional lattices with four components*, Phys. Rev. **64**, 178 (1943), doi:10.1103/PhysRev.64.178.

[14] R. V. Ditzian, J. R. Banavar, G. S. Grest and L. P. Kadanoff, *Phase diagram for the Ashkin-Teller model in three dimensions*, Phys. Rev. B **22**, 2542 (1980), doi:10.1103/PhysRevB.22.2542.

[15] J. Sólyom, *Duality of the block transformation and decimation for quantum spin systems*, Phys. Rev. B **24**, 230 (1981), doi:10.1103/PhysRevB.24.230.

[16] M. Kohmoto, M. den Nijs and L. P. Kadanoff, *Hamiltonian studies of the d = 2 Ashkin-Teller model*, Phys. Rev. B **24**, 5229 (1981), doi:10.1103/PhysRevB.24.5229.

[17] S. Jin, A. Sen and A. W. Sandvik, *Ashkin-Teller criticality and pseudo-first-order behavior in a frustrated Ising model on the square lattice*, Phys. Rev. Lett. **108**, 045702 (2012), doi:10.1103/PhysRevLett.108.045702 [preprint doi:10.48550/arXiv.1110.5874].

[18] S. Jin, A. Sen, W. Guo and A. W. Sandvik, *Phase transitions in the frustrated Ising model on the square lattice*, Phys. Rev. B **87**, 144406 (2013), doi:10.1103/PhysRevB.87.144406 [preprint doi:10.48550/arXiv.1212.5339].

[19] A. Udupa, S. Sur, S. Nandy, A. Sen and D. Sen, *Weak universality, quantum many-body scars, and anomalous infinite-temperature autocorrelations in a one-dimensional spin model with duality*, Phys. Rev. B **108**, 214430 (2023), doi:10.1103/physrevb.108.214430 [preprint doi:10.48550/arXiv.2307.11161].

[20] A. O'Brien, S. D. Bartlett, A. C. Doherty and S. T. Flammia, *Symmetry-respecting real-space renormalization for the quantum Ashkin-Teller model*, Phys. Rev. E **92**, 042163 (2015), doi:10.1103/PhysRevE.92.042163 [preprint doi:10.48550/arXiv.1507.00038].

[21] J. C. Bridgeman, A. O'Brien, S. D. Bartlett and A. C. Doherty, *Multiscale entanglement renormalization Ansatz for spin chains with continuously varying criticality*, Phys. Rev. B **91**, 165129 (2015), doi:10.1103/PhysRevB.91.165129 [preprint doi:10.48550/arXiv.1501.02817].

[22] I. Sau, A. Sen and D. Banerjee, *Weak universality induced by Q = ±2e charges at the deconfinement transition of a (2 + 1)-dimensional U(1) lattice gauge theory*, Phys. Rev. Lett. **130**, 071901 (2023), doi:10.1103/PhysRevLett.130.071901 [preprint doi:10.48550/arXiv.2209.14606].

[23] R. Dijkgraaf, E. Verlinde and H. Verlinde, *C = 1 conformal field theories on Riemann surfaces*, Commun. Math. Phys. **115**, 649 (1988), doi:10.1007/BF01224132.

[24] S.-K. Yang, *Modular invariant partition function of the Ashkin-Teller model on the critical line and N = 2 superconformal invariance*, Nucl. Phys. B **285**, 183 (1987), doi:10.1016/0550-3213(87)90334-8.

[25] C. Holzhey, F. Larsen and F. Wilczek, *Geometric and renormalized entropy in conformal field theory*, Nucl. Phys. B **424**, 443 (1994), doi:10.1016/0550-3213(94)90402-2.

[26] P. Calabrese and J. Cardy, *Entanglement entropy and quantum field theory*, J. Stat. Mech.: Theory Exp. P06002 (2004), doi:10.1088/1742-5468/2004/06/P06002.

[27] H. Bernien et al., *Probing many-body dynamics on a 51-atom quantum simulator*, Nature **551**, 579 (2017), doi:10.1038/nature24622 [preprint doi:10.48550/arXiv.1707.04344].

[28] S. Ebadi et al., *Quantum phases of matter on a 256-atom programmable quantum simulator*, Nature **595**, 227 (2021), doi:10.1038/s41586-021-03582-4.

[29] D. Bluvstein et al., *Controlling quantum many-body dynamics in driven Rydberg atom arrays*, Science **371**, 1355 (2021), doi:10.1126/science.abg2530 [preprint doi:10.48550/arXiv.2012.12276].

[30] G. Semeghini et al., *Probing topological spin liquids on a programmable quantum simulator*, Science **374**, 1242 (2021), doi:10.1126/science.abi8794 [preprint doi:10.48550/arXiv.2104.04119].

[31] C. J. Turner, A. A. Michailidis, D. A. Abanin, M. Serbyn and Z. Papić, *Weak ergodicity breaking from quantum many-body scars*, Nat. Phys. **14**, 745 (2018), doi:10.1038/s41567-018-0137-5.

[32] K. Bull, I. Martin and Z. Papić, *Systematic construction of scarred many-body dynamics in 1D lattice models*, Phys. Rev. Lett. **123**, 030601 (2019), doi:10.1103/PhysRevLett.123.030601 [preprint doi:10.48550/arXiv.1903.10491].

[33] V. Khemani, C. R. Laumann and A. Chandran, *Signatures of integrability in the dynamics of Rydberg-blockaded chains*, Phys. Rev. B **99**, 161101 (2019), doi:10.1103/PhysRevB.99.161101 [preprint doi:10.48550/arXiv.1807.02108].

[34] C. Danieli, A. Andreanov, D. Leykam and S. Flach, *Flat band fine-tuning and its photonic applications*, Nanophotonics **13**, 3925 (2024), doi:10.1515/nanoph-2024-0135.

[35] R. Moessner and S. L. Sondhi, *Ising models of quantum frustration*, Phys. Rev. B **63**, 224401 (2001), doi:10.1103/PhysRevB.63.224401 [preprint doi:10.48550/arXiv.cond-mat/0011250].

[36] D. S. Rokhsar and S. A. Kivelson, *Superconductivity and the quantum hard-core dimer gas*, Phys. Rev. Lett. **61**, 2376 (1988), doi:10.1103/PhysRevLett.61.2376.

[37] A. Chattopadhyay, B. Mukherjee, K. Sengupta and A. Sen, *Strong Hilbert space fragmentation via emergent quantum drums in two dimensions*, SciPost Phys. **14**, 146 (2023), doi:10.21468/SciPostPhys.14.6.146 [preprint doi:10.48550/arXiv.2208.13800].

[38] J. R. Schrieffer and P. A. Wolff, *Relation between the Anderson and Kondo Hamiltonians*, Phys. Rev. **149**, 491 (1966), doi:10.1103/PhysRev.149.491.

[39] S. Bravyi, D. P. DiVincenzo and D. Loss, *Schrieffer-Wolff transformation for quantum many-body systems*, Ann. Phys. **326**, 2793 (2011), doi:10.1016/j.aop.2011.06.004 [preprint doi:10.48550/arXiv.1105.0675].

[40] S. Sachdev, *Quantum phase transitions*, Cambridge University Press, Cambridge, UK, ISBN 9780521514682 (2011), doi:10.1017/CBO9780511973765.

[41] B. Mukherjee, S. Nandy, A. Sen, D. Sen and K. Sengupta, *Collapse and revival of quantum many-body scars via Floquet engineering*, Phys. Rev. B **101**, 245107 (2020), doi:10.1103/PhysRevB.101.245107 [preprint doi:10.48550/arXiv.1907.08212].

[42] B. Mukherjee, A. Sen, D. Sen and K. Sengupta, *Dynamics of the vacuum state in a periodically driven Rydberg chain*, Phys. Rev. B **102**, 075123 (2020), doi:10.1103/PhysRevB.102.075123 [preprint doi:10.48550/arXiv.2005.07715].

[43] G. von Gehlen and V. Rittenberg, *The Ashkin-Teller quantum chain and conformal invariance*, J. Phys. A: Math. Gen. **20**, 227 (1987), doi:10.1088/0305-4470/20/1/030.

[44] C. Lannert, M. P. A. Fisher and T. Senthil, *Quantum confinement transition in a d-wave superconductor*, Phys. Rev. B **63**, 134510 (2001), doi:10.1103/PhysRevB.63.134510 [preprint doi:10.48550/arXiv.cond-mat/0007002].

[45] L. Balents, L. Bartosch, A. Burkov, S. Sachdev and K. Sengupta, *Putting competing orders in their place near the Mott transition*, Phys. Rev. B **71**, 144508 (2005), doi:10.1103/PhysRevB.71.144508 [preprint doi:10.48550/arXiv.cond-mat/0408329].

[46] S. Sachdev, K. Sengupta and S. M. Girvin, *Mott insulators in strong electric fields*, Phys. Rev. B **66**, 075128 (2002), doi:10.1103/PhysRevB.66.075128 [preprint doi:10.48550/arXiv.cond-mat/0205169].

[47] P. Fendley, K. Sengupta and S. Sachdev, *Competing density-wave orders in a one-dimensional hard-boson model*, Phys. Rev. B **69**, 075106 (2004), doi:10.1103/PhysRevB.69.075106 [preprint doi:10.48550/arXiv.cond-mat/0309438].

[48] Z. Yan, Y. Wu, C. Liu, O. F. Syljuåsen, J. Lou and Y. Chen, *Sweeping cluster algorithm for quantum spin systems with strong geometric restrictions*, Phys. Rev. B **99**, 165135 (2019), doi:10.1103/PhysRevB.99.165135 [preprint doi:10.48550/arXiv.1809.05792].

[49] N. Chepiga and F. Mila, *DMRG investigation of constrained models: From quantum dimer and quantum loop ladders to hard-boson and Fibonacci anyon chains*, SciPost Phys. **6**, 033 (2019), doi:10.21468/SciPostPhys.6.3.033 [preprint doi:10.48550/arXiv.1809.00746].

[50] P. Lajkó and F. Iglói, *Numerical study of the critical behavior of the Ashkin-Teller model at a line defect*, J. Stat. Mech.: Theory Exp. P05025 (2011), doi:10.1088/1742-5468/2011/05/P05025.

[51] G. Duchowney, C. Naón and A. Iucci, *Critical behavior of the Ashkin-Teller model with a line defect: Towards reconciliation between numerical and analytical results*, Phys. A: Stat. Mech. Appl. **597**, 127287 (2022), doi:10.1016/j.physa.2022.127287.